



# Consistent diffusivity measurement between Galvanostatic Intermittent Titration Technique and Electrochemical Impedance Spectroscopy

Changyu Deng<sup>a</sup>, Wei Lu<sup>a,b,\*</sup>

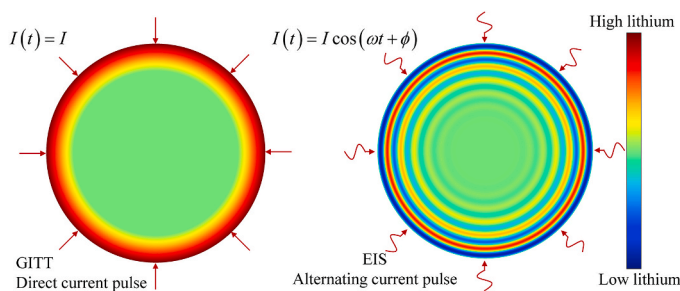
<sup>a</sup> Department of Mechanical Engineering, University of Michigan, Ann Arbor, MI, 48109, United States

<sup>b</sup> Department of Materials Science & Engineering, University of Michigan, Ann Arbor, MI, 48109, United States

## HIGHLIGHTS

- Diffusion models of GITT and EIS are analyzed for various particle shape and size.
- Explained why the two techniques often give large difference in measured diffusivity.
- Identical results when current excitation does not impact deep inside the particles.
- An EIS approach to measure diffusivity independent of particle size or geometry.
- Short impulse time and high frequency reduce measurement inconsistency.

## GRAPHICAL ABSTRACT



## ARTICLE INFO

### Keywords:

Lithium ion battery  
Diffusivity  
Galvanostatic intermittent titration technique  
Electrochemical impedance spectroscopy

## ABSTRACT

Galvanostatic Intermittent Titration Technique (GITT) and Electrochemical Impedance Spectroscopy (EIS) are two popular methods to measure the diffusivity of lithium ions in electrode particles. What has puzzled the community for a long time is that these two techniques often give an order of magnitude difference in the results. By analyzing the diffusion profile and approximation error for various particle geometries, we show that these two techniques are consistent only when the current excitation does not impact deep inside the particles, which corresponds to the condition of short pulse time for GITT or high frequency for EIS. GITT does not depend on particle size by its assumption while EIS does. Thus we propose an innovative approach of using EIS to determine diffusivity accurately independent of particle size or geometry. We further demonstrate experimentally that the two techniques yield identical results under the right measurement conditions. This work may provide insight on the scattering of measured diffusivity data in the literature.

## 1. Introduction

Accurate measurement of lithium ion diffusivity in electrode particles is essential for analyzing and predicting battery performance. Galvanostatic Intermittent Titration Technique (GITT) and Electrochemical

Impedance Spectroscopy (EIS) are the two most widely used techniques. For GITT, a current pulse is applied to the cell and diffusivity is calculated by the slope of voltage response as a function of the square root of time. For EIS, the cell is connected to an alternating current (AC) source and the impedance is measured as a function of the current frequency.

\* Corresponding author. Department of Mechanical Engineering, University of Michigan, Ann Arbor, MI, 48109, United States.

E-mail address: [weilu@umich.edu](mailto:weilu@umich.edu) (W. Lu).

<https://doi.org/10.1016/j.jpowsour.2020.228613>

Received 22 April 2020; Received in revised form 30 June 2020; Accepted 3 July 2020

Available online 5 August 2020

0378-7753/© 2020 Elsevier B.V. All rights reserved.

The diffusivity is obtained by fitting the impedance data to a model, such as the semi-infinite solid diffusion model [1] or the equivalent circuit model [2].

There have been numerous experiments using these two techniques. However, what has puzzled the community for a long time is that these two techniques often give an order of magnitude difference in the results [3–5]. Various explanations have been proposed to explain the discrepancy, such as the fitting error of EIS [6], invalid uniform current assumption of GITT [6,7], or different impact of ohmic resistance on GITT [8]. However, no detailed theoretical analysis or experimental verification has been provided.

In this paper, we propose an explanation to the cause of large difference in the measured diffusivity obtained by GITT and EIS. By analyzing diffusion in a plate, in a cylinder and in a sphere, we correlate the diffusion characteristics to the GITT and EIS conditions. We investigate the error from approximation and assumptions on which these two techniques are based. We show that the two methods are consistent only when the current excitation influences a shallow layer into the particle surface. We then demonstrate experimentally that the two methods indeed give consistent results under the right experimental conditions. The difference of measured diffusivity between the two methods is only about 10% on average.

## 2. Model

The formulas of GITT and EIS are based on diffusion models. In this section, we derive the expressions of diffusivity for different particle geometries and perform error analysis of the two techniques.

### 2.1. Analysis of GITT

GITT assumes that the current on the particle surface is uniform and diffusion is one-dimensional. Let us consider the diffusion of Li ions in a plate, in a cylinder and in a sphere, as shown in Fig. 1. The particle is at equilibrium before the current pulse. With Fick's law, the ion concentration can be written as

$$\frac{\partial c}{\partial t} = \frac{1}{x^{d-1}} D \frac{\partial}{\partial x} \left( x^{d-1} \frac{\partial c}{\partial x} \right), \quad (1)$$

where  $x$  is the coordinate measured from the symmetry line,  $t$  is time,  $D$  is the diffusion coefficient in the electrode particle, and  $d$  is the dimension number (1 for planar, 2 for cylindrical and 3 for spherical particles). For simple notation, here  $c(x,t)$  refers to the change of concentration from the initial equilibrium uniform distribution. So we have

$$c(x, 0) = 0. \quad (2)$$

The boundary condition at the symmetry line ( $x = 0$ ) is given by

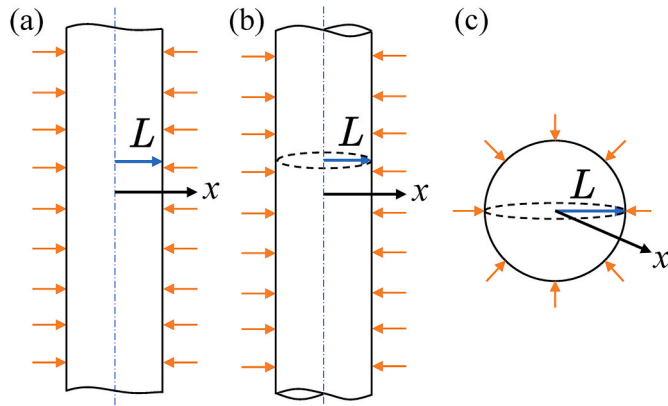


Fig. 1. Schematic of lithium ion intercalation into a (a) plate, (b) cylinder, (c) sphere.

$$\left. \frac{\partial c}{\partial x} \right|_{x=0} = 0. \quad (3)$$

The other boundary, exposed to the electrolyte, has a given ion influx caused by the current,

$$D \left. \frac{\partial c}{\partial x} \right|_{x=L} = \frac{I}{SFz} \quad (4)$$

where  $I$  denotes the total current,  $S$  is the total surface area,  $z$  is the charge number of ions (1 for lithium) and  $F$  is Faraday constant.

For a plate ( $d = 1$ ), the ion concentration at the surface of the particle ( $x = L$ ) can be obtained by solving Eqs. (1)–(4) using series [9], which gives

$$c(L, t) = \frac{2I\sqrt{t}}{SFz\sqrt{D}} \sum_{n=0}^{\infty} \left[ \operatorname{ierfc} \left( \frac{nL}{\sqrt{Dt}} \right) + \operatorname{ierfc} \left( \frac{(n+1)L}{\sqrt{Dt}} \right) \right], \quad (5)$$

where  $\operatorname{ierfc}(x) = e^{-x^2}/\sqrt{\pi} - \operatorname{xerfc}(x)$  is the first integral of the complement of the error function. When  $t \ll L^2/D$ , the term  $x = nL/\sqrt{Dt}$  approaches infinity for  $n \geq 1$ . Note that  $\lim_{x \rightarrow +\infty} \operatorname{ierfc}(x) = 0$ , so we can ignore the  $n \geq 1$  terms. Consider the  $n = 0$  term and  $\operatorname{ierfc}(0) = 1/\sqrt{\pi}$ . The equation becomes

$$c(L, t) = \frac{2I\sqrt{t}}{SFz\sqrt{\pi D}}. \quad (6)$$

The solution to a cylinder ( $d = 2$ ) is more complicated. To the leading order terms [9], we can write the solution as

$$c(L, t) = \frac{I}{SFzD} \left[ 2\sqrt{\frac{Dt}{\pi}} + \frac{2Dt}{\sqrt{\pi}L} + o \left( \left( \frac{Dt}{L^2} \right)^{3/2} \right) \right]. \quad (7)$$

When  $t \ll L^2/D$ , the second and higher order terms of  $\sqrt{Dt}/L$  can be neglected. The equation reduces to Eq. (6).

The solution to a spherical particle can be written as (see Appendix A for details)

$$c(L, t) = \frac{IL}{SFzD} \left( \frac{2}{\sqrt{\pi}} \frac{\sqrt{Dt}}{L} + o \left( \frac{Dt}{L^2} \right) \right). \quad (8)$$

When  $t \ll L^2/D$ , we can neglect the higher order term on the right, and the equation reduces to Eq. (6).

It is not a coincidence that the ion concentration at the surface follows the same expression of Eq. (6) for the three very different geometries, as long as  $t \ll L^2/D$ . The proportionality to square root of time comes from the solution of ion diffusion into a semi-infinite plane, whose exact analytical form is given by Eq. (6). When the time is short ( $t \ll L^2/D$ ), diffusion only penetrates into a thin layer near the surface of particles regardless of the particle geometry. Therefore, they all show the same form of Eq. (6).

It is more convenient to use stoichiometry,  $\delta$  ( $0 \leq \delta \leq 1$ ), instead of ion concentration in application. We have

$$dc = \frac{d\delta}{V_M}, \quad (9)$$

where  $V_M$  is the molar volume of the sample. The state that we can measure directly from the cell is its voltage. Take the derivative of Eq. (6) with respect to  $\sqrt{t}$  and combine it with Eq. (9), we have

$$D = \frac{4}{\pi} \left( \frac{IV_M}{SFz} \right)^2 \left[ \left( \frac{dU^0}{d\delta} \right) / \left( \frac{dV}{d\sqrt{t}} \right) \right]^2 \quad (10)$$

where  $V$  is the cell voltage as a function of time  $t$  after the current pulse,  $dU^0/d\delta$  denotes the derivative of the open circuit voltage with respect to stoichiometry or state of charge (SOC) when the full stoichiometry window is used.  $U^0$  as a function of  $\delta$  can be measured from the voltage

at each steady state (i.e. lithium ion concentration is uniform in the particle) of a half-cell during the rest period between pulses. Besides SI units, it is common to use centimeter as the length scale so that the units are  $V_M$  in  $[\text{cm}^3 \cdot \text{mol}^{-1}]$ ,  $S$  in  $[\text{cm}^2]$  and  $D$  in  $[\text{cm}^2 \cdot \text{s}^{-1}]$ .

Although Eq. (10) was originally derived for a dense planar electrode [10], our derivation and analysis above show that the equation holds for all shapes of particles as long as  $t \ll L^2/D$ .

If time  $t$  is not small enough to satisfy  $t \ll L^2/D$ , applying Eq. (10) will introduce some error. To understand how large the error could be, we performed two types of numerical simulations. Firstly, we solved the diffusion model described by Eqs. (1)–(4) using the finite element method (FEM) to obtain the concentration  $c(L,t)$  for a preset diffusivity value. Then we used Eq. (6), i.e. the analytical solution for  $t \ll L^2/D$ , to estimate diffusivity based on the solved concentration. The relative error of estimation was then calculated by the absolute difference between the estimated diffusivity and the preset diffusivity divided by the preset diffusivity value. Secondly, we used the pseudo two-dimensional (P2D) electrochemical model to simulate a lithium-graphite cell and recorded the voltage response to a current pulse (see Appendix B for details). Based on the voltage profile, we estimated diffusivity using Eq. (10). Then the relative error of estimation was calculated.

Fig. 2 shows the relative error of diffusivity estimation. At the beginning of the pulse ( $tD/L^2 < 10^{-5}$ ), the error is large due to capacitive effects as well as limitation of resolution in simulation. When time is large ( $tD/L^2 > 10^{-3}$ ), the curves from diffusion and P2D models match perfectly, showing that the error originates from the approximation by Eq. (6). Now we recommend the appropriate measurement condition using the curve of sphere since it has the largest error among the three geometries. For the error to be less than 20%,  $tD/L^2$  should be less than  $4 \times 10^{-3}$ . For the error to be less than 10%,  $tD/L^2$  needs to be less than  $10^{-3}$ . In a typical graphite electrode ( $D = 10^{-14} \text{ m}^2 \text{ s}^{-1}$ ,  $L = 10^{-5} \text{ m}$ ), these translate to a requirement of measurement within 40 s and 10 s after the pulse, respectively. For an electrode containing particles of different sizes, calculating the maximum time (estimating diffusivity must use the data within this time for accuracy) should consider smaller particle sizes. For instance, one can take  $L$  to be the mean radius minus a standard deviation.

## 2.2. Analysis of EIS

EIS measures the cell impedance by applying an alternating current (AC) with a sinusoidal waveform. The impedance of a Li-ion cell, in a simple equivalent circuit model, is interpreted to consist of solution

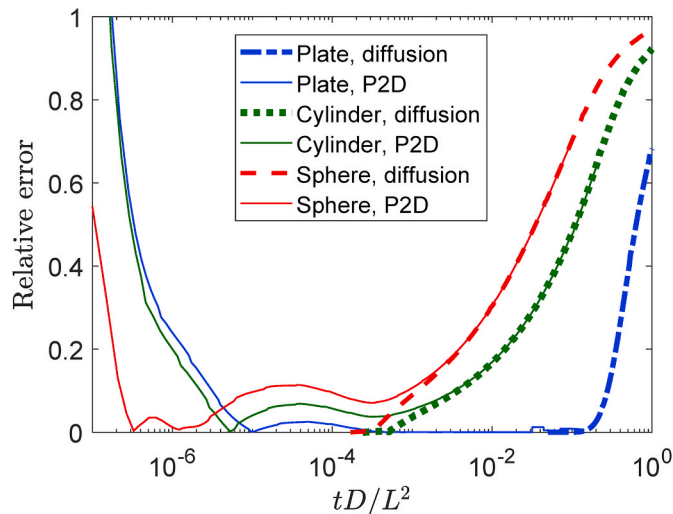


Fig. 2. Relative error of diffusivity estimation, calculated from diffusion and P2D models.

resistance, charge transfer resistance and diffusion impedance (also known as Warburg impedance) [11]. Here we focus on diffusion impedance which is relevant to diffusivity in the electrode particles. The governing equation of diffusion under AC is the same as Eq. (1). The boundary condition of symmetry in Eq. (2) holds as well, but the other boundary condition in Eq. (4) is no longer a constant flux. Instead, the current  $I$  should be replaced by  $I(t) = |I| \cos(\omega t + \varphi)$ , where  $\omega$  is the angular frequency and  $\varphi$  is the phase angle. The initial condition in Eq. (2) is no longer relevant since we care about the steady state response, where the cell voltage is also a cosine wave of the same angular frequency but with a different phase angle.

The impedance of the cell by EIS is calculated from voltage divided by current. Based on the results in the literature [11], we organize the expressions of diffusion impedance in Table 1. In the expressions,  $i$  is the unit imaginary number, and  $I_0$  and  $I_1$  are modified Bessel functions of the first kind.

The solutions of EIS have closed forms rather than infinite series of GITT. However, EIS requires prior knowledge of particle geometries to choose the correct equation and to determine the length  $L$ . A common method is to assume that all particles have the same shape and size, such as spherical particles, and fit the parameter  $L$  [6]. However, in a real electrode, the shapes of the particles are not the same and their sizes are not uniform. The variance of particles has a large impact on the impedance curves, as will be shown later.

The asymptotic approximations give a concise form of impedance when we ignore the error up to  $O((\sqrt{D/\omega L^2})^3)$ , but  $L$  is still in the expressions for cylindrical ( $d = 2$ ) and spherical ( $d = 3$ ) particles, indicating an impact of particle geometry. It is worthy to note that if we ignore errors up to  $O(D/\omega L^2)$ , solutions for all the three geometries can be approximated by

$$Z = \frac{dU^0}{d\delta} \frac{V_M}{SF\sqrt{2D\omega}} (1 - i), \quad (11)$$

which is a  $45^\circ$  line on the Nyquist plot. Interestingly, the impedance form in Eq. (11) is independent of length scale or particle geometry. From a physical point of view, when the frequency is high, only the concentration at particle surface is influenced by the AC. This situation is the same as that in GITT. Mathematically, Eq. (11) should work well on estimating the diffusivity without the need to consider particle geometry. In practice, however, the condition  $\omega \gg D/L^2$  is not easy to satisfy. This is because the high frequency region is dominated by capacitance and charge transfer, while the diffusion region normally appears at low frequency in the spectrum. As a result, we often only see a very short segment with a  $45^\circ$  angle, or even the angle of the line is not  $45^\circ$  at all on the Nyquist plot.

An innovative approach we propose here is to use the real part of the asymptotic approximations which is independent of length  $L$ . This approach does not require a segment of  $45^\circ$  angle line on the Nyquist plot or even the existence of a straight segment. The proposed formula to obtain diffusivity is

$$D = \frac{1}{2} \left( \frac{dU^0}{d\delta} \frac{V_M}{SF} \right)^2 \left( \frac{d \operatorname{Re}(Z)}{d \sqrt{1/\omega}} \right)^{-2} \quad (12)$$

We can plot  $\operatorname{Re}(Z)$  as a function of  $\sqrt{1/\omega}$  and calculate diffusivity based on the slope, instead of using the average of real and imaginary parts [5] or an arbitrarily one of them [1].

By comparing the estimated diffusivity using Eq. (12) with that from the exact solutions, we can investigate the estimation error. The results are shown in Fig. 3, where the relative error is defined as the absolute difference between the estimated diffusivity and that calculated from the exact solutions, divided by that from the exact solutions. Similar to GITT in Fig. 1, sphere has the largest error among the three shapes, so we use its curve to recommend measurement conditions. For instance,  $\omega L^2/D = 80$  and  $43$  correspond to 10% and 20% error, respectively. For a

**Table 1**  
Solutions of impedance  $Z$  and asymptotic approximations.

| $d$          | Exact solution  | Asymptotic approximation ( $\omega \gg D/L^2$ )  |
|--------------|---|--|
| 1 (plate)    | $\frac{dU^0}{d\delta} \frac{V_M L}{SFD} \frac{\coth(\sqrt{i\omega L^2/D})}{\sqrt{i\omega L^2/D}}$                               | $\frac{dU^0}{d\delta} \frac{V_M}{SF\sqrt{2D\omega}} (1 - i)$   |
| 2 (cylinder) | $\frac{dU^0}{d\delta} \frac{V_M L}{SFD} \frac{I_0(\sqrt{i\omega L^2/D})}{\sqrt{i\omega L^2/D} I_1(\sqrt{i\omega L^2/D})}$       | $\frac{dU^0}{d\delta} \frac{V_M}{SF} \left[ \frac{1}{\sqrt{2D\omega}} (1 - i) - \frac{1}{2\omega L} i \right]$ |
| 3 (sphere)   | $\frac{dU^0}{d\delta} \frac{V_M L}{SFD} \frac{\tanh(\sqrt{i\omega L^2/D})}{\sqrt{i\omega L^2/D} - \tanh(\sqrt{i\omega L^2/D})}$ | $\frac{dU^0}{d\delta} \frac{V_M}{SF} \left[ \frac{1}{\sqrt{2D\omega}} (1 - i) - \frac{1}{\omega L} i \right]$  |

typical graphite electrode ( $D = 10^{-14} \text{ m}^2 \text{ s}^{-1}$ ,  $L = 10^{-5} \text{ m}$ ), these translate to a requirement of frequency higher than 0.08 Hz and 0.04 Hz, respectively. For an electrode containing particles of different sizes,  $L$  should be chosen as the small particle radius to more accurately calculate the requirement. The large error corresponds to the region that  $d \text{Re}(Z)/d \sqrt{1/\omega}$  is not a constant. In practical measurement, we can confirm that the frequency is sufficient (not too low) by observing that the  $\text{Re}(Z) \sim \sqrt{1/\omega}$  curve appears as a straight line.

Practically, the particle size in an electrode is not uniform. For instance, particles in a graphite electrode whose median radius is  $8.7 \mu\text{m}$  can range from  $0.01 \mu\text{m}$  to  $100 \mu\text{m}$  and particles in a  $\text{LiNi}_{0.4}\text{Co}_{0.6}\text{O}_2$  electrode whose median radius is  $6.5 \mu\text{m}$  can range from  $0.01 \mu\text{m}$  to  $50 \mu\text{m}$  [6]. To show how the particle size impacts impedance and how our method can eliminate the impact, we assume that the particle radius,  $\hat{L}$ , has a bilinear distribution in  $[0.5L, 1.5L]$ , where  $L$  is the mean radius. The probability density function is

$$f(\hat{L}) = \begin{cases} \frac{2}{L} - \frac{4}{L} \frac{|\hat{L} - L|}{L} - 1, & |\hat{L} - L| \leq 0.5L \\ 0, & |\hat{L} - L| > 0.5L \end{cases} \quad (13)$$

Then we can treat  $\hat{L}$  as a random variable and calculate the corresponding impedance from the exact solution by the equations in Table 1. The results are presented in the left column of Fig. 4. The exact solution depends on  $\hat{L}$  so it appears as a band. The approximate solution is calculated using Eq. (11), which is independent of  $\hat{L}$  and therefore it appears as a curve. The impedance of spherical particles has a wide band, meaning that its impedance is highly sensitive to the particle size.

The relative error between the impedance calculated from  $\hat{L}$  and that from the mean radius,  $L$ , is defined by

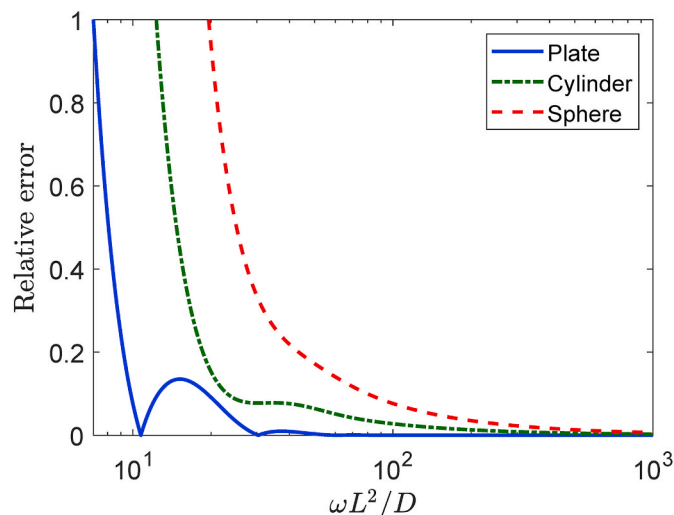


**Fig. 3.** Relative error of diffusivity estimation using Eq. (12).

$$\text{Error}(\omega) = \left| \frac{Z^*(\hat{L}, \omega) - Z^*(L, \omega)}{Z^*(L, \omega)} \right|, \quad (14)$$

where  $Z^*$  denotes the real part or the imaginary part of impedance  $Z$ . For exact solutions,  $Z^*(\hat{L}, \omega)$  is a function of  $\hat{L}$ , thus it forms an error band. By contrast, the approximate solution is calculated using Eq. (11) which is independent of particle size, therefore, the error for approximate solution shows as a curve.

It is interesting to note that although the approximate solution introduces some truncation error relative to the exact solution, the approximate solution performs better for diffusion estimation than the exact solution. This is because the particle size has a distribution in the electrode. Using the exact solution requires selecting a particle shape and size. However, as shown in the right column of Fig. 4, the error band is very broad. One particle size cannot represent the size distribution, and selecting the wrong size can lead to large estimation error. By contrast, the approximate solution eliminates any size and shape dependence. After ensuring sufficient frequency (e.g.  $\omega L^2/D = 100$ ), the approximate solution gives very small error. It can be observed that the real part of the impedance spectrum is more accurate than the imaginary part when estimating diffusivity. For example, Fig. 4d and f show that the error of real part is only 6.3% and 8.9% of that of the imaginary part when  $\omega L^2/D = 100$ . Our approach is based on the real part of the spectrum, therefore gives high accuracy. In addition, our approach eliminates the particle shape effect, which further reduces the error.

### 3. Experimental characterization

In the previous section, we showed from the theoretical models and simulations that EIS and GITT are consistent when only a thin layer near the surface is impacted. Namely, the time of current impulse for GITT should be short ( $t \ll L^2/D$ ) and the frequency of EIS should be high ( $\omega \gg D/L^2$ ). When these conditions are met, the results from the two methods should be consistent.

To verify our claim, we compare the two methods by measuring the diffusivity of graphite particles in a lithium-graphite cell.

#### 3.1. Cell fabrication

We made CR2032 coin cells with lithium metal and graphite as two electrodes. Graphite powder (MTI, 80 wt%) was mixed with polyvinylidene fluoride (PVDF) binder (10 wt%), super P (10 wt%) and 1-Methyl-2-pyrrolidone to make a homogeneous slurry. The slurry was pasted on  $9 \mu\text{m}$ -thick Cu foil (MTI) and vacuum-dried at  $110^\circ\text{C}$  for 12 h. The electrode sheet whose mass loading was about  $4 \text{ mg cm}^{-2}$  was cut into circular discs. Next, graphite electrode pieces were assembled to sealed 2032 type coin cells with a lithium metal (Sigma Aldrich) counter electrode and a separator (Celgard 2320) in an argon-filled glove box (MBraun) containing less than 0.1 ppm oxygen and moisture. The electrolyte solution was 1 M lithium hexafluorophosphate solution ( $\text{LiPF}_6$ ) dissolved in a mixture (1:1, v/v) of ethylene carbonate (EC) and dimethyl carbonate (DMC, premixed solution from Sigma Aldrich).

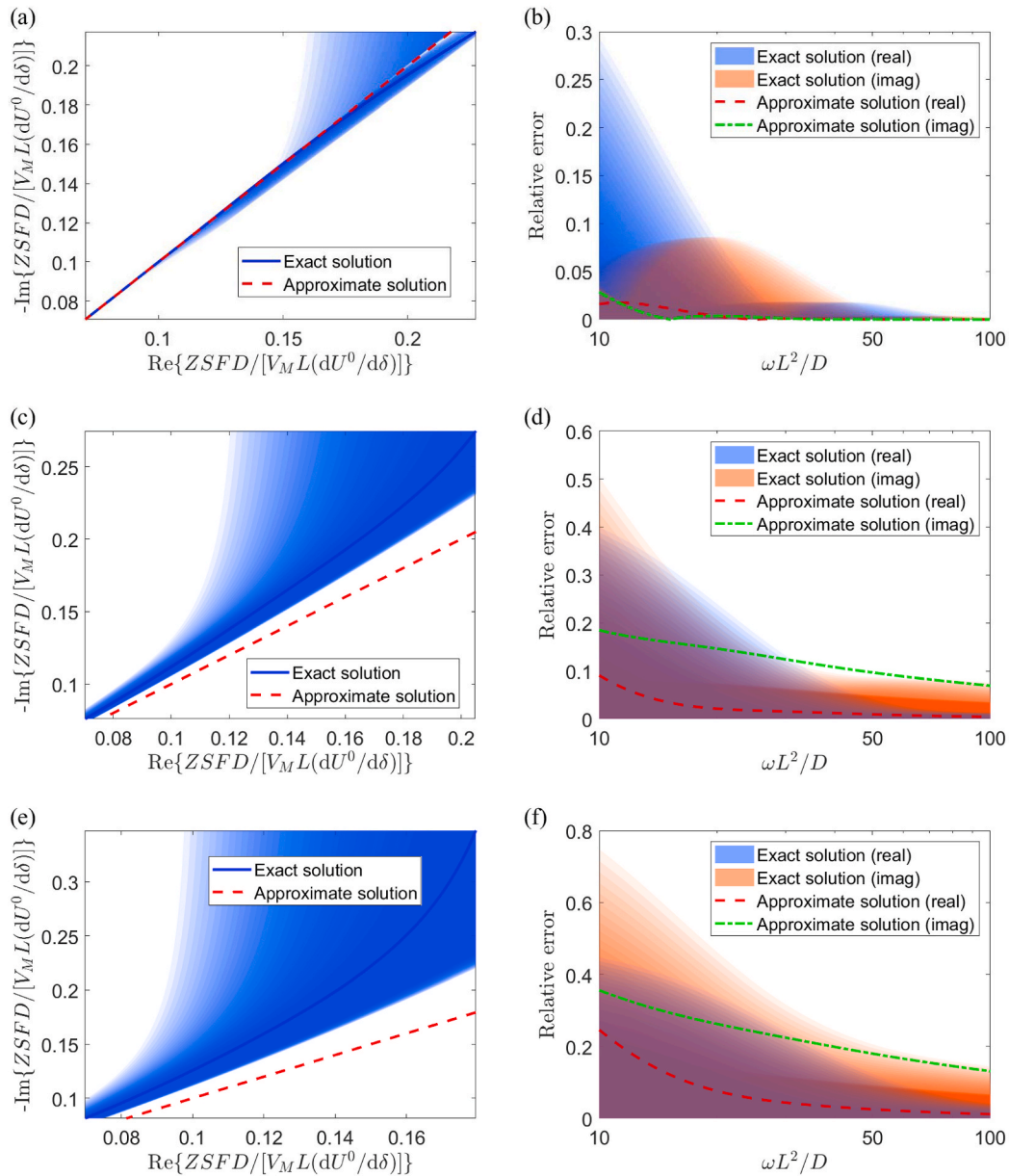


**Fig. 4.** Left column: impedance from the exact solutions (appears as a band because of particle size distribution) and from the approximate solution of Eq. (11) (appears as a curve because of independence on particle size). The blue curve indicates the impedance curve at  $\hat{L} = L$ . The shade reflects probability, with darker for higher probability. Right column: relative error of diffusivity estimation for distributed particle sizes. The shade reflects probability. Results for particle shape of (a, b) plate, (c, d) cylinder, (e, f) sphere. (For interpretation of the references to colour in this figure legend, the reader is referred to the Web version of this article.)

### 3.2. Measurement

An assembled cell was first cycled at  $50 \text{ mA g}^{-1}_{\text{graphite}}$  for 10 cycles between 0.01 V and 1.5 V to stabilize its performance. Before measurement, the cell was rested for at least 12 hours for it to reach equilibrium. EIS testing was performed by connecting the cell to a VersaSTAT4 electrochemical workstation controlled by a computer. Next, the cell was rested for an hour to reach equilibrium, removing any disturbance by the EIS test. The cell was then connected to a computer-controlled MACCOR cycler with a pulse charging (graphite deintercalation) current of  $50 \text{ mA g}^{-1}_{\text{graphite}}$  for GITT. At this stage, a pair of EIS/GITT tests were completed. We performed tests on three cells, and performed three pairs of tests for each cell at various states of charge (total 9 pairs).

### 4. Results

Fig. 5 shows an example of line fitting to calculate diffusivity from both methods. In Fig. 5a,  $t = 0$  corresponds to the beginning of the pulse. Our purpose for this experiment is to compare the results from the two methods, so we normalize diffusivity by

$$\bar{D} = \frac{D}{\left(\frac{dU^0}{d\delta} \frac{V_M}{SF}\right)^2}, \quad (15)$$

since diffusivity from both methods are proportional to the denominator in Eq. (15). Consequently, there is no need to measure these parameters. The difference between GITT and EIS is less than 8%.

Fig. 6 shows the results for nine test pairs (Fig. 5 corresponds to the left pair of Cell 3). In our tests, the range of time is about 1 s–10 s and the

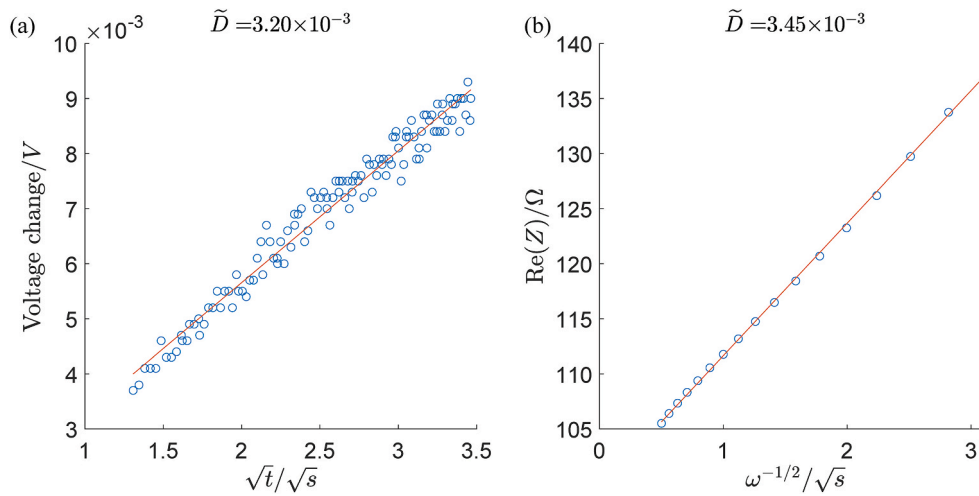


Fig. 5. Fitting the slopes for (a) GITT and (b) EIS.

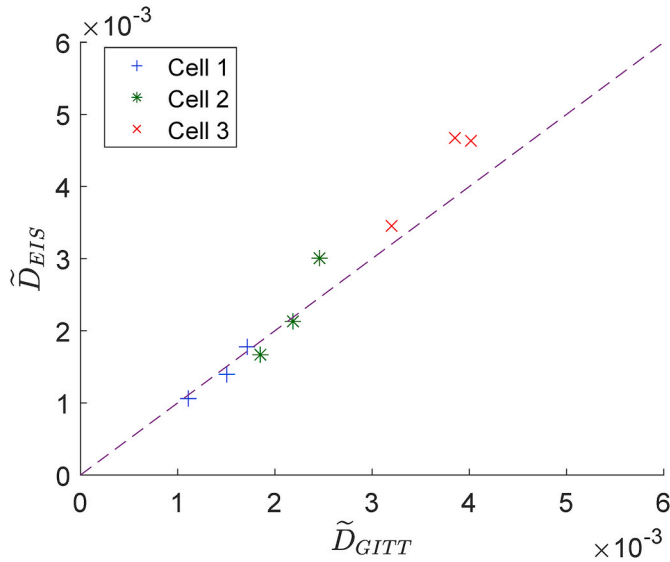


Fig. 6. Normalized diffusivity of nine test pairs from three different cells at various states of charge. The dash line indicates identical diffusivity results from GITT and EIS.

range of frequency is about 0.1 Hz–10 Hz, although they vary with cells and test conditions. We can observe that all points line up along the dash line, indicating that the results from GITT and EIS are consistent. The average difference between GITT and EIS results is only about 10%.

5. Conclusions

This work aims to explain the discrepancy of diffusivity measured by GITT and EIS. With analytical forms for various particle geometries, we showed that the condition of GITT ( $t \ll L^2/D$ ) makes the result insensitive to the particle size or shape. By contrast, the curve at the diffusion region, i.e., at low frequency, of EIS is determined by particle size distribution and their shapes. We proposed an approach using the real part of the impedance so that the measured diffusivity is independent of particle size or geometry. We conducted an experiment to measure the diffusivity in graphite particles, which confirmed that the two methods gave consistent results with only 10% difference on average. In summary, the major factors causing the discrepancy between the measured diffusivity from GITT and EIS in the literature are:

1. The short after-pulse time requirement of GITT. There is a trade-off when selecting the data to analyze after the current pulse. If the data is at a time too short after the pulse, other types of resistance, such as charge transfer, plays an important role. If the data is at a time too long after the pulse, the equation for GITT, Eq. (10), is not valid. As shown in Fig. 2, a good strategy is to keep  $tD/L^2 \sim 10^{-4}$  or less while making sure that the data exhibits a linear relation between voltage and the square root of time.
2. The impact of particle geometry on EIS. The typical lower bound of the frequency in EIS tests is 1–10 mHz, thus concentration fluctuation might occur deep inside the particles. The shape and size variance of particles play a large role (Fig. 4), but they are commonly ignored. We found that the frequency should be high (e.g,  $\omega L^2/D > 80$ ) but cannot go beyond the diffusion region. We also propose to use Eq. (12) instead of exact solutions to eliminate any dependence on particle shape and size. In fact, because of particle shape and size distribution in an electrode, exact solutions often lead to poor estimation. Using the exact solutions requires selecting a particle shape and size, however, one size cannot represent the size distribution, and selecting the wrong size can give very wrong results.
3. Fitting error of the equivalent circuit model. In many EIS tests, diffusivity is obtained together with other parameters, such as charge transfer resistance, by fitting the entire impedance data to an equivalent circuit model. Such fitting is not easy to control and may cause a large error of diffusivity since it suffers from the errors of trying to fit other parameters and their parts of the curve (e.g. the semi-circle part). Therefore, we propose to use only the real part of the impedance at a given range (high frequency in the diffusion region) to simplify the fitting process to linear regression. Our method could eliminate the error of other fitting parameters.

CRediT authorship contribution statement

**Changyu Deng:** Formal analysis, Methodology, Investigation, Data curation, Visualization, Writing - original draft. **Wei Lu:** Conceptualization, Methodology, Writing - review & editing, Resources, Funding acquisition, Supervision.

Declaration of competing interest

The authors declare that they have no known competing financial interests or personal relationships that could have appeared to influence the work reported in this paper.

**Acknowledgement**

The authors gratefully acknowledge the support by the National Science Foundation under Grant No. CNS-1446117 and by LG Chem. We

thank Chenhe Zhang for the helpful discussion on the math of differential equations and Andrew Kim for the help with experimental equipment setup.

**Appendix A. derivation of Eq. (8)**

Let  $u = cx$ , from Eq. (1) with  $d = 3$  we have

$$\frac{\partial u}{\partial t} = D \frac{\partial^2 u}{\partial x^2}. \tag{A1}$$

The initial condition in Eq. (2) becomes

$$u(x, 0) = 0. \tag{A2}$$

The boundaries conditions are

$$u(0, t) = 0, \tag{A3}$$

$$\left. \frac{\partial u}{\partial x} \right|_{x=L} = \frac{IL}{SFzD} + \frac{u(L, t)}{L}. \tag{A4}$$

Such a problem can be solved by Laplace transform,

$$U(x, s) = L[u(x, t)] = \int_0^\infty e^{-st} u(x, t) dt. \tag{A5}$$

The governing equation and boundary conditions become

$$sU = D \frac{\partial^2 U}{\partial x^2}, \tag{A6}$$

$$U(0, s) = 0, \tag{A7}$$

$$\left. \frac{\partial U}{\partial x} \right|_{x=L} = \frac{IL}{sSFzD} + \frac{U(L, s)}{L}. \tag{A8}$$

The general solution to (A6) yields

$$U = C_1 \sinh(\sqrt{s/D}x) + C_2 \cosh(\sqrt{s/D}x). \tag{A9}$$

With the application of boundary conditions, we have

$$U = \frac{IL \sinh(\sqrt{s/D}x)}{sSFzD \left[ \sqrt{s/D} \cosh(\sqrt{s/D}L) - \sinh(\sqrt{s/D}L) / L \right]}. \tag{A10}$$

To approximate the function at a short time after the pulse, we reformulate the equation to

$$U = \frac{IL \left( e^{\sqrt{s/D}x} - e^{-\sqrt{s/D}x} \right)}{sSFzD \left[ \sqrt{s/D} \left( e^{\sqrt{s/D}L} + e^{-\sqrt{s/D}L} \right) - \left( e^{\sqrt{s/D}L} - e^{-\sqrt{s/D}L} \right) / L \right]} = \frac{IL \left( e^{-(L-x)\sqrt{s/D}} - e^{-(L+x)\sqrt{s/D}} \right)}{sSFzD \left( \sqrt{s/D} + \sqrt{s/D} e^{-2L\sqrt{s/D}} - 1 / L + e^{-2L\sqrt{s/D}} / L \right)}$$

$$= \frac{IL \left( e^{-(L-x)\sqrt{s/D}} - e^{-(L+x)\sqrt{s/D}} \right)}{sSFzD \left( \sqrt{s/D} - 1 / L \right)} \left[ \frac{1}{1 + \frac{\sqrt{s/D} + 1/L}{\sqrt{s/D} - 1/L} e^{-2L\sqrt{s/D}}} \right] = \frac{IL \left( e^{-(L-x)\sqrt{s/D}} - e^{-(L+x)\sqrt{s/D}} \right)}{sSFzD \left( \sqrt{s/D} - 1 / L \right)} \sum_{n=0}^\infty \left[ (-1)^n \left( \frac{\sqrt{s/D} + 1/L}{\sqrt{s/D} - 1/L} \right)^n e^{-2L\sqrt{s/D}n} \right] \tag{A11}$$

Note that  $e^{-2L\sqrt{s/D}n}$  decays exponentially with  $\sqrt{s}$  unless  $n = 0$  in the series. Since  $t$  approaching 0 corresponds to  $s$  approaching infinity [12], we can ignore the terms of  $n \geq 1$  to get

$$U = \frac{IL \left( e^{-(L-x)\sqrt{s/D}} - e^{-(L+x)\sqrt{s/D}} \right)}{sSFzD \left( \sqrt{s/D} - 1 / L \right)}. \tag{A12}$$

By using the formula  $L^{-1} \left[ \frac{ae^{-k\sqrt{s}}}{s(a+\sqrt{s})} \right] = -e^{ak+a^2t} \operatorname{erfc} \left( a\sqrt{t} + \frac{k}{2\sqrt{t}} \right) + \operatorname{erfc} \left( \frac{k}{2\sqrt{t}} \right)$  [12], we have

$$u = \frac{IL^2}{SFzD} \left\{ \left[ e^{-\frac{(L-x)\sqrt{D}t}{L} + \frac{D}{L^2}t} \operatorname{erfc} \left( -\frac{\sqrt{Dt}}{L} + \frac{L-x}{2\sqrt{Dt}} \right) - \operatorname{erfc} \frac{L-x}{2\sqrt{Dt}} \right] - \left[ e^{-\frac{(L+x)\sqrt{D}t}{L} + \frac{D}{L^2}t} \operatorname{erfc} \left( -\frac{\sqrt{Dt}}{L} + \frac{L+x}{2\sqrt{Dt}} \right) - \operatorname{erfc} \frac{L+x}{2\sqrt{Dt}} \right] \right\}. \tag{A13}$$

Converting it back by  $c = u/x$  and plug in  $x = L$ , we have

$$c(L, t) = \frac{IL}{SFzD} \left\{ \left[ e^{\frac{D}{L^2}t} \operatorname{erfc}\left(-\frac{\sqrt{Dt}}{L}\right) - 1 \right] - \left[ e^{-2+\frac{D}{L^2}t} \operatorname{erfc}\left(-\frac{\sqrt{Dt}}{L} + \frac{L}{\sqrt{Dt}}\right) - \operatorname{erfc}\frac{L}{\sqrt{Dt}} \right] \right\}. \quad (\text{A14})$$

With  $\sqrt{Dt}/L \ll 1$ , we have

$$c(L, t) = \frac{IL}{SFzD} \left[ e^{\frac{D}{L^2}t} \operatorname{erfc}\left(\frac{\sqrt{Dt}}{L}\right) + O\left(\frac{Dt}{L^2}\right) \right] = \frac{IL}{SFzD} \left[ \left(1 + \frac{D}{L^2}t\right) \left(\frac{2}{\sqrt{\pi}} \frac{\sqrt{Dt}}{L}\right) + O\left(\frac{Dt}{L^2}\right) \right] = \frac{IL}{SFzD} \left( \frac{2}{\sqrt{\pi}} \frac{\sqrt{Dt}}{L} + O\left(\frac{Dt}{L^2}\right) \right) \quad (\text{A15})$$

## Appendix B. pseudo two-dimensional model

Pseudo two-dimensional (P2D) model is widely used to simulate Li-ion batteries. There are numerous papers related to this model, e.g. Ref. [13, 14]. Here we only introduce the model briefly. We consider a half cell composed of lithium metal, separator and graphite electrode. The diffusion in the active material particle (graphite) is given by

$$\frac{\partial c_s}{\partial t} = \frac{D_s}{r^2} \frac{\partial}{\partial r} \left( r^2 \frac{\partial c_s}{\partial r} \right), \quad (\text{B1})$$

where  $c_s$  is the lithium ion concentration in the solid and  $r$  is the radial coordinate. The solid potential,  $\Phi_s$ , is governed by

$$\frac{\partial}{\partial x} \left( \sigma_{s,eff} \frac{\partial \Phi_s}{\partial x} \right) = a_s j, \quad (\text{B2})$$

where  $x$  is the coordinate along electrode thickness,  $\sigma_{s,eff} = \sigma_s \varepsilon_s^{1.5}$  is the effective solid conductivity with  $\sigma_s$  being the bulk solid conductivity and  $\varepsilon_s$  being the volume fraction of solid,  $a_s = 3\varepsilon_s/r_p$  is the active surface area per unit volume with  $r_p$  being the particle radius, and  $j$  denotes the current density.

The lithium ion concentration in the electrolyte,  $c_e$ , is given by

$$\varepsilon_e \frac{\partial c_e}{\partial t} + \frac{\partial}{\partial x} \left( -D_{e,eff} \frac{\partial c_e}{\partial x} \right) = \frac{(1-t_+)}{F} a_s j, \quad (\text{B3})$$

where  $D_{e,eff} = D_e \varepsilon_e^{1.5}$  is the effective electrolyte diffusivity with  $D_e$  being the bulk electrolyte diffusivity and  $\varepsilon_e$  being the volume fraction of electrolyte, and  $t_+$  is the lithium ion transference number. The electrolyte potential,  $\Phi_e$ , is governed by

$$\frac{\partial}{\partial x} \left\{ -\kappa_{e,eff} \left[ \frac{\partial \Phi_e}{\partial x} - \frac{2RT}{F} \left( 1 + \frac{d \ln f_{\pm}}{d \ln c_e} \right) (1-t_+) \frac{\partial \ln c_e}{\partial x} \right] \right\} = a_s j, \quad (\text{B4})$$

where  $\kappa_{e,eff} = \kappa_e \varepsilon_e^{1.5}$  is the effective electrolyte conductivity with  $\kappa_e$  being the bulk electrolyte conductivity,  $R$  is gas constant,  $T$  is temperature, and  $f_{\pm}$  is the electrolyte activity coefficient.

The current density between the solid and the electrolyte is governed by the Butler-Volmer equation

$$j = i_0 \left\{ \exp \left[ \frac{\alpha F (\eta - j r_{film})}{RT} \right] - \exp \left[ -\frac{(1-\alpha) F (\eta - j r_{film})}{RT} \right] \right\}, \quad (\text{B5})$$

where  $i_0$  is the exchange current density,  $\alpha$  is the anodic charge transfer coefficient,  $r_{film}$  is the film resistance (such as SEI) and  $\eta$  is the over-potential calculated by

$$\eta = \Phi_s - \Phi_e - U^0, \quad (\text{B6})$$

where  $U^0$  is the equilibrium potential of graphite material.

In the separator domain, Eqs. (B3) and (B4) still hold except that  $j = 0$ .

Major parameters used in our simulations are listed in Table B1.

**Table B1**  
Major parameters used in the P2D simulation

| Symbol                | Description                                       | Value                  |
|-----------------------|---|------------------------|
| $L_{neg}$             | Graphite electrode thickness                      | $5 \times 10^{-5}$ m   |
| $L_{sep}$             | Separator thickness                               | $2 \times 10^{-5}$ m   |
| $\varepsilon_{s,neg}$ | Solid volume fraction in graphite electrode       | 0.3                    |
| $\varepsilon_{e,neg}$ | Electrolyte volume fraction in graphite electrode | 0.6                    |
| $\varepsilon_{e,sep}$ | Electrolyte volume fraction in separator          | 0.4                    |
| $i_{0,neg}$           | Exchange current density for graphite             | $30 \text{ A m}^{-2}$  |
| $i_{0,Li}$            | Exchange current density for lithium metal        | $100 \text{ A m}^{-2}$ |

(continued on next page)



Table B1 (continued)

| Symbol         | Description   | Value  |
|----------------|---|--|
| $r_{film,neg}$ | Surface film resistance of graphite particles                         | $0.1 \Omega \text{ m}^2$                       |
| $dU^0/d\delta$ | Derivative of the open circuit voltage with respect to stoichiometry  | 2 V  |
| $D_s$          | Graphite particle diffusivity   | $2 \times 10^{-15} \text{ m}^2 \text{ s}^{-1}$ |
| $\sigma_s$     | Graphite conductivity   | $100 \text{ S m}^{-1}$                         |
| $c_{e0}$       | Initial electrolyte concentration                                     | $1000 \text{ mol m}^{-3}$                      |
| $r_p$          | Graphite particle radius  | $10^{-5} \text{ m}$                            |
| $j_{Li}$       | Current density at Li metal surface, equal to applied current density | $1 \text{ A m}^{-2}$                           |

The equations above are solved by the finite element method using COMSOL Multiphysics 5.4. Other parameters take the default values in the COMSOL material database.

## References

- [1] C. Ho, I. Raistrick, R. Huggins, Application of A-C techniques to the study of lithium diffusion in tungsten trioxide thin films, *J. Electrochem. Soc.* 127 (1980) 343–350.
- [2] Q.-C. Zhuang, X.-Y. Qiu, S.-D. Xu, Y.-H. Qiang, S.-G. Sun, Diagnosis of Electrochemical Impedance Spectroscopy in Lithium-ion Batteries, *InTechOpen*, 2012, pp. 189–227.
- [3] S. Yang, X. Wang, X. Yang, Y. Bai, Z. Liu, H. Shu, Q. Wei, Determination of the chemical diffusion coefficient of lithium ions in spherical  $\text{Li}[\text{Ni}_{0.5}\text{Mn}_{0.3}\text{Co}_{0.2}]\text{O}_2$ , *Electrochim. Acta* 66 (2012) 88–93, <https://doi.org/10.1016/j.electacta.2012.01.061>.
- [4] Y. Bai, X. Wang, X. Zhang, H. Shu, X. Yang, B. Hu, Q. Wei, H. Wu, Y. Song, The kinetics of Li-ion deintercalation in the Li-rich layered  $\text{Li}_{1.12}[\text{Ni}_{0.5}\text{Co}_{0.2}\text{Mn}_{0.3}]\text{O}_{2.89}$  studied by electrochemical impedance spectroscopy and galvanostatic intermittent titration technique, *Electrochim. Acta* 109 (2013) 355–364, <https://doi.org/10.1016/j.electacta.2013.06.134>.
- [5] K.M. Shaju, G.V.S. Rao, B.V.R. Chowdari, Electrochemical kinetic studies of Li-ion in  $\text{O}_2$ -structured  $\text{Li}_{2/3}(\text{Ni}_{1/3}\text{Mn}_{2/3})\text{O}_2$  and  $\text{Li}_{2/3+x}(\text{Ni}_{1/3}\text{Mn}_{2/3})\text{O}_2$  by EIS and GITT, *J. Electrochem. Soc.* 150 (2003) A1, <https://doi.org/10.1149/1.1521754>.
- [6] M. Ecker, T.K.D. Tran, P. Dechent, S. Käbitz, A. Warnecke, D.U. Sauer, Parameterization of a physico-chemical model of a lithium-ion battery I. Determination of parameters, *J. Electrochem. Soc.* 162 (2015) A1836–A1848, <https://doi.org/10.1149/2.0551509jes>.
- [7] D.W. Dees, S. Kawauchi, D.P. Abraham, J. Prakash, Analysis of the galvanostatic intermittent titration technique (GITT) as applied to a lithium-ion porous electrode, *J. Power Sources* 189 (2009) 263–268, <https://doi.org/10.1016/j.jpowsour.2008.09.045>.
- [8] M. Levi, D. Aurbach, Frumkin intercalation isotherm—a tool for the description of lithium insertion into host materials: a review, *Electrochim. Acta* 45 (1999) 167–185, [https://doi.org/10.1016/s0013-4686\(99\)00202-9](https://doi.org/10.1016/s0013-4686(99)00202-9).
- [9] H.S. Carslaw, J.C. Jaeger, *Conduction of Heat in Solids*, second ed., vol. 310, Clarendon Press, Oxford, 1959, p. 75, 331.
- [10] W. Weppner, Determination of the kinetic parameters of mixed-conducting electrodes and application to the system  $\text{Li}_3\text{Sb}$ , *J. Electrochem. Soc.* 124 (1977) 1569, <https://doi.org/10.1149/1.2133112>.
- [11] J. Song, M.Z. Bazant, Effects of nanoparticle geometry and size distribution on diffusion impedance of battery electrodes, *J. Electrochem. Soc.* 160 (2012) A15–A24, <https://doi.org/10.1149/2.023301jes>.
- [12] D.W. Hahn, M.N. Ozisik, *Heat Conduction*, John Wiley & Sons, Inc., Hoboken, New Jersey, 2012, pp. 371–388.
- [13] A. Jokar, B. Rajabloo, M. Désilets, M. Lacroix, Review of simplified Pseudo-two-Dimensional models of lithium-ion batteries, *J. Power Sources* 327 (2016) 44–55, <https://doi.org/10.1016/j.jpowsour.2016.07.036>.
- [14] B. Wu, W. Lu, A battery model that fully couples mechanics and electrochemistry at both particle and electrode levels by incorporation of particle interaction, *J. Power Sources* 360 (2017) 360–372, <https://doi.org/10.1016/j.jpowsour.2017.05.115>.